PHILOSOPHICAL TRANSACTIONS OF THE ROYAL SOCIETY A

rsta.royalsocietypublishing.org

Research

Cite this article: Beare RJ, Cullen MJP. 2013 Diagnosis of boundary-layer circulations. Phil Trans R Soc A 371: 20110474.
http://dx.doi.org/10.1098/rsta.2011.0474

One contribution of 13 to a Theme Issue 'Mathematics applied to the climate system'.

Subject Areas:
atmospheric science

Keywords:
boundary layer, circulation, Ekman balance, advection, Sawyer–Eliassen equation, low-level jet

Author for correspondence:
Robert J. Beare
e-mail: r.j.beare@exeter.ac.uk

Royal Society Publishing
Informing the science of the future

Diagnosis of boundary-layer circulations

Robert J. Beare[1] and Michael J. P. Cullen[2]

[1]Departments of Mathematics and Computer Science, CEMPS, University of Exeter, Harrison Building, North Park Road, Exeter EX4 4QF, UK
[2]Met Office, FitzRoy Road, Exeter EX1 3PB, UK

Diagnoses of circulations in the vertical plane provide valuable insights into aspects of the dynamics of the climate system. Dynamical theories based on geostrophic balance have proved useful in deriving diagnostic equations for these circulations. For example, semi-geostrophic theory gives rise to the Sawyer–Eliassen equation (SEE) that predicts, among other things, circulations around mid-latitude fronts. A limitation of the SEE is the absence of a realistic boundary layer. However, the coupling provided by the boundary layer between the atmosphere and the surface is fundamental to the climate system. Here, we use a theory based on Ekman momentum balance to derive an SEE that includes a boundary layer (SEEBL). We consider a case study of a baroclinic low-level jet. The SEEBL solution shows significant benefits over Ekman pumping, including accommodating a boundary-layer depth that varies in space and structure, which accounts for buoyancy and momentum advection. The diagnosed low-level jet is stronger than that determined by Ekman balance. This is due to the inclusion of momentum advection. Momentum advection provides an additional mechanism for enhancement of the low-level jet that is distinct from inertial oscillations.

1. Introduction

The climate system consists of phenomena on a large range of spatial and temporal scales. In climate models, spatial scales that are resolved by the grid scale can typically be represented by its advective dynamics. In addition, there is a large range of important processes with scales smaller than the grid scale; examples of these processes are: radiation, moist convection, land-surface heterogeneity and boundary-layer turbulence.

These processes are represented by sub-grid parametrizations. A challenge for climate modellers is understanding the coupling between the sub-grid parametrizations and the resolved dynamics. It is arguable that such coupling has received much less research effort relative to the separate development of the dynamical core and parametrizations. Here, we focus around the important case of the coupling between the atmosphere and the ocean or land surface. This is very important, and is achieved primarily through heat, moisture and momentum transfers within the atmospheric boundary layer.

Our approach to understanding the coupling between the dynamics and the boundary layer is to consider regimes where the two are close to a state of balance. Our understanding of the large-scale atmosphere and ocean circulations has been greatly helped by the realization that they are close to a state of geostrophic balance (pressure gradients balancing Coriolis force). The quasi-, semi- and planetary geostrophic models extend the steady-state balance assumptions to include non-stationarity and advection. Following the seminal works of Eliassen [1] and Sawyer [2], the Sawyer–Eliassen equation (SEE) diagnoses the ageostrophic circulations forced by advection of heat and momentum. The SEE has proved invaluable in describing the dynamics of meteorological fronts. Subsequently, Hoskins [3] defined the semi-geostrophic (SG) theory, from which the SEE can be derived.

A weakness of the SEE is that it lacks a representation of the atmospheric boundary layer. Inclusion of the effects of turbulent diffusion would thus be valuable in understanding the coupling between the boundary-layer parametrization and the dynamics in both climate and weather prediction models. The aim of this paper is to form a diagnostic Sawyer–Eliassen equation including a boundary layer (SEEBL) for circulations in the vertical plane. Analogous to the SEE, we will assume that the boundary layer is close to a state of balance, but now we use the Ekman balance (pressure gradient, Coriolis force and boundary-layer drag in balance). Such a balance has been used in diagnosing Ekman pumping for cyclone systems [4] or ocean gyres and convergence in the tropics [5]. However, the extension to include non-stationarity and advection has been less used. Beare & Cullen [6,7] demonstrated the use of time-varying models based on Ekman balance for stratified and shallow water systems, respectively. They also demonstrated the utility of the semi-geotriptic (SGT) model, directly analogous to the SG model, but with a realistic boundary layer included.

Low-level jets are a significant feature of atmospheric behaviour. They contribute to extremes such as very high winds in extra-tropical cyclones [8] and heavy rainfall [9]. Low-level jets also feature a combination of dynamical, moisture and boundary-layer forcings. It is typically observed that low-level jets have a significant ageostrophic component [10]. Here, we will aim to expand on this observation by using a theory that defines the dynamics relative to the Ekman-balanced wind rather than the geostrophic wind.

First, we will derive the SGT equations from the primitive equations, also describing the regime for which they are valid (§2). In §3, the SEEBL will then be derived from the SGT equations. We will then give example numerical solutions of the SEEBL for a mid-latitude low-level jet, and show the benefits of this new equation in describing the coupling to the interior dynamics.

2. The semi-geotriptic equations

In this section, we derive the SGT equations that are the basis of the SEEBL diagnostic circulation equation.

(a) Primitive equations including boundary-layer parametrization

We start our analysis with the two-dimensional, Boussinesq, hydrostatic primitive equations (HPEs) on an f-plane, including boundary-layer terms:

$$\frac{\mathrm{D}u}{\mathrm{D}t} - fv + \frac{\partial \phi}{\partial x} = \frac{\partial}{\partial z}\left(K_\mathrm{m}\frac{\partial u}{\partial z}\right), \tag{2.1}$$

Table 1. Symbols used in equations (2.1)–(2.6). All variables are a function of (x, z, t).

symbol	meaning
(x, z, t)	Cartesian coordinates and time
(u, v, w)	wind vector
f	Coriolis parameter (constant)
ϕ	geopotential
b	buoyancy
K_m	boundary-layer vertical momentum diffusivity
K_h	boundary-layer vertical thermal diffusivity
F_b	boundary-layer buoyancy tendency

$$\frac{\mathrm{D}v}{\mathrm{D}t} + fu = \frac{\partial}{\partial z}\left(K_m \frac{\partial v}{\partial z}\right), \tag{2.2}$$

$$\frac{\partial \phi}{\partial z} = b, \tag{2.3}$$

$$\frac{\mathrm{D}b}{\mathrm{D}t} = \frac{\partial}{\partial z}\left(K_h \frac{\partial b}{\partial z}\right) = F_b, \tag{2.4}$$

$$\frac{\partial u}{\partial x} + \frac{\partial w}{\partial z} = 0 \tag{2.5}$$

and

$$\frac{\mathrm{D}}{\mathrm{D}t} = \frac{\partial}{\partial t} + u\frac{\partial}{\partial x} + w\frac{\partial}{\partial z}. \tag{2.6}$$

The symbols used above are defined in table 1. The terms on the right-hand side of equations (2.1), (2.2) and (2.4) represent the forcing due to the boundary layer. The boundary layer is represented by vertical diffusion terms on the basis that the boundary-layer depth is much less than the horizontal scale of interest. Here, we confine our analysis to stratified and near-neutral flows in the boundary layer. We use a first-order closure for stratified and near-neutral boundary layers used in many numerical weather prediction models [11]. Here, the vertical diffusivities of momentum and heat are expressed as a function of a mixing length (λ), the vertical wind shear (S) and functions of gradient Richardson number (Ri):

$$K_m = \lambda^2 S f_m(Ri) \quad \text{and} \quad K_h = \lambda^2 S f_h(Ri), \tag{2.7}$$

where f_m and f_h are stability functions for momentum and heat, respectively. The boundary-layer mixing is controlled by the 'long-tails' function, which has the form

$$f_m(Ri) = Pr f_h(Ri) = \frac{1}{1 + 10Ri}, \quad Ri \geq 0, \quad Pr = 0.7, \tag{2.8}$$

where Pr is the neutral Prandtl number. While many theoretical studies assume that K_m is constant, here, we use a realistic diffusivity, which is a function of both space and time.

(b) Ekman balance limit of hydrostatic primitive equations

Given a boundary-layer frictional time scale, τ_f, and the advective time scale, T, we can define a small dimensionless parameter, ϵ:

$$\epsilon = \frac{\min[f^{-1}, \tau_f]}{T}. \tag{2.9}$$

The min operation is designed to capture the faster process out of the Coriolis and the boundary-layer friction. In the limit of zero ϵ, advection is negligible with respect to the Coriolis, pressure-gradient and boundary-layer friction forces in equations (2.1) and (2.2), giving the

zero-order Ekman balance:

$$-fv_e + \frac{\partial \phi}{\partial x} = \frac{\partial}{\partial z}\left(K_m \frac{\partial u_e}{\partial z}\right) \tag{2.10}$$

and

$$fu_e = \frac{\partial}{\partial z}\left(K_m \frac{\partial v_e}{\partial z}\right). \tag{2.11}$$

The components of the Ekman-balanced wind are u_e and v_e (hence the subscript 'e'). The Ekman-balanced wind is also sometimes called the 'geotriptic' (Earth rubbing) wind. When the boundary-layer momentum diffusivity is zero, equations (2.10) and (2.11) revert to geostrophic balance, so also apply above the boundary layer.

The frictional thermal wind balance in the x direction is formed by taking $\partial/\partial z$ of equation (2.10) and substituting for $\partial\phi/\partial z$ from equation (2.3):

$$f\frac{\partial v_e}{\partial z} - \frac{\partial b}{\partial x} = -\mathcal{D}\frac{\partial u_e}{\partial z}, \tag{2.12}$$

where the vertical diffusion operator, $\mathcal{D}$, applied to an an arbitrary function, g, is written as $\mathcal{D}g = (\partial^2/\partial z^2)(K_m g)$.

(c) Derivation of semi-geotriptic equations

We now consider the case where ϵ is *non-zero* and advection is no longer negligible. We expand the horizontal winds in equations (2.1) and (2.2) as an asymptotic expansion in ϵ about Ekman balance:

$$\left.\begin{aligned} u &= u_e + u_1 + O(\epsilon^2 u_e), \\ v &= v_e + v_1 + O(\epsilon^2 v_e) \\ \text{and} \quad |u_1| &= \epsilon|u_e|, \quad |v_1| = \epsilon|v_e|. \end{aligned}\right\} \tag{2.13}$$

The terms in equations (2.13) are expressed as successive powers of ϵ. Substituting equations (2.13) into equations (2.1) and (2.2) and retaining terms of order $\epsilon|u_e|$ and $\epsilon|v_e|$ respectively gives

$$\frac{Du_e}{Dt} - f(v - v_e) = \frac{\partial}{\partial z}\left(K_m \frac{\partial (u - u_e)}{\partial z}\right) \tag{2.14}$$

and

$$\frac{Dv_e}{Dt} + f(u - u_e) = \frac{\partial}{\partial z}\left(K_m \frac{\partial (v - v_e)}{\partial z}\right). \tag{2.15}$$

While this is typically the endpoint of the analysis for asymptotic expansion about the geostrophic wind [12], there is an additional important consideration of stability when Ekman balance is used. For the approximation to be useful, it is necessary that equations (2.14) and (2.15) can be solved for $O(T\epsilon^{-1})$, long time, so that accuracy can be maintained. While the diffusive terms in equations (2.14) and (2.15) are second-order accurate in ϵ, they lead to an unstable evolution of the domain integrated energy (E_{int}) in the absence of heating ($F_b = 0$):

$$\frac{dE_{int}}{dt} = -\int_0^{H_d}\int_{-L_d}^{L_d} K_m \left[2\frac{\partial u}{\partial z}\frac{\partial u_e}{\partial z} + 2\frac{\partial v}{\partial z}\frac{\partial v_e}{\partial z} - \left(\frac{\partial u_e}{\partial z}\right)^2 - \left(\frac{\partial v_e}{\partial z}\right)^2\right] dx\, dz \tag{2.16}$$

and

$$E_{int} = \int_0^{H_d}\int_{-L_d}^{L_d}\left[\frac{1}{2}(u_e^2 + v_e^2) - zb\right] dx\, dz, \tag{2.17}$$

where the domain width and height are $2L_d$ and H_d, respectively. The right-hand side of equation (2.16) is dependent on both (u, v) as well as (u_e, v_e), meaning that the energy evolution will not be robustly negative definite. For example, when $\partial u/\partial z$ and $\partial u_e/\partial z$ have opposite signs, E_{int} could grow instead of decay. Beare & Cullen [7] provide more analysis of this situation.

In order to maintain a negative definite energy tendency, the sign of the diffusive term needs to be reversed, giving the SGT equations:

$$\frac{\mathrm{D}u_\mathrm{e}}{\mathrm{D}t} - f(v - v_\mathrm{e}) = \frac{\partial}{\partial z}\left(K_\mathrm{m}\frac{\partial(u_\mathrm{e} - u)}{\partial z}\right) \tag{2.18}$$

and

$$\frac{\mathrm{D}v_\mathrm{e}}{\mathrm{D}t} + f(u - u_\mathrm{e}) = \frac{\partial}{\partial z}\left(K_\mathrm{m}\frac{\partial(v_\mathrm{e} - v)}{\partial z}\right). \tag{2.19}$$

We note that the advecting wind (u) has a significant divergent component, including the Ekman-balanced wind u_e, so none of the terms in the thermodynamic equations can be neglected. The buoyancy equation used is thus

$$\frac{\mathrm{D}b}{\mathrm{D}t} = F_\mathrm{b}. \tag{2.20}$$

The domain integrated energy in the absence of heating is now negative definite:

$$\frac{\mathrm{d}E_\mathrm{int}}{\mathrm{d}t} = -\int_0^{H_\mathrm{d}}\int_{-L_\mathrm{d}}^{L_\mathrm{d}} K_\mathrm{m}\left[\left(\frac{\partial u_\mathrm{e}}{\partial z}\right)^2 + \left(\frac{\partial v_\mathrm{e}}{\partial z}\right)^2\right]\mathrm{d}x\,\mathrm{d}z. \tag{2.21}$$

This means that the second-order accuracy of equations (2.14) and (2.15) cannot be maintained in time, but first-order accuracy of equations (2.18) and (2.19) can be maintained, so that diagnostics calculated from them will be meaningful. The inclusion of advection and inertial terms on the left-hand side of equations (2.18) and (2.19) and buoyancy advection in equation (2.20) still gives an improvement in accuracy over simply using Ekman balance [7]. The SGT equations are also only accurate in the region of the boundary layer where Ekman balance is a good first approximation, above the surface layer (approximately the lowest 10% of the boundary layer).

(d) Relationship to geostrophic models

Given that L and U are typical scales for length and horizontal velocity respectively and assuming that τ_f^{-1} is negligible above the boundary layer gives

$$\epsilon = \frac{1}{fT} = \frac{U}{fL} = Ro, \tag{2.22}$$

where Ro is the Rossby number. The appropriate zero-order balance is now geostrophic. Figure 1 compares both geostrophic and Ekman balances. When the advection of buoyancy and momentum is significant, we form the prognostic equations given in the second row of figure 1; the prognostic equations based on geostrophic balance are the familiar planetary, SG and quasi-geostrophic equations. The SGT equations are the Ekman-balanced analogue of the SG equations. The reasons for this particular analogue in the boundary layer, as opposed to the quasi-geostrophic analogue, is that the SG thermodynamic equation includes all the advection terms.

3. Sawyer–Eliassen equation including the boundary layer (SEEBL)

The SEE is a linear diagnostic equation for the ageostrophic wind derived from the semi-geostrophic equations [1,2]. In an analogous way, we will derive an SEE including a boundary layer using the SGT equations. We apply frictional thermal wind balance (equation (2.12)) to

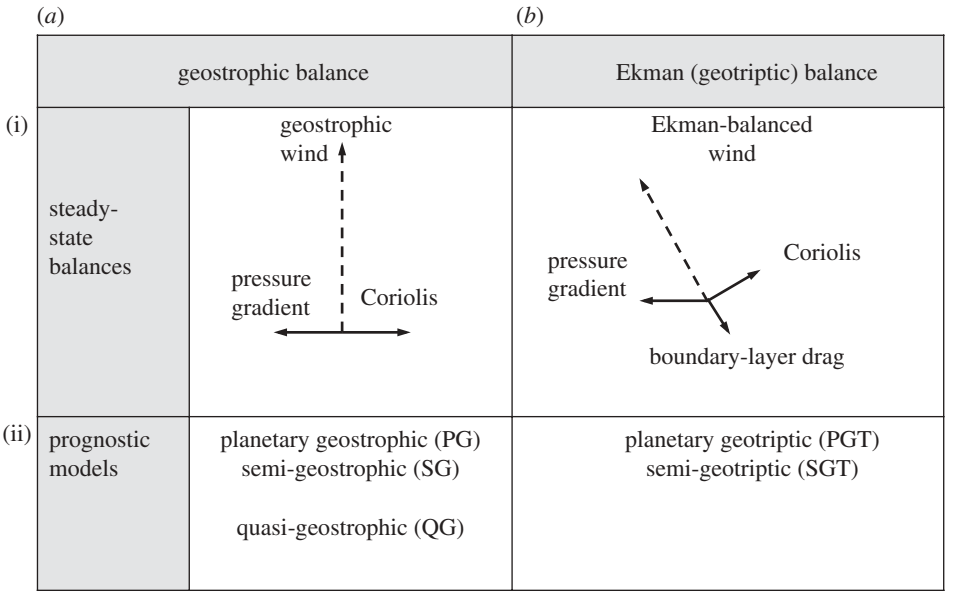

Figure 1. The balances (*a*) above and (*b*) within the boundary layer. (i) The steady-state balances, and (ii) the associated time-varying balanced models described in §2.

equations (2.18)–(2.20) in order to eliminate the time derivatives of u_e, v_e and b. The resulting SEEBL is

$$\left[f\left(f+\frac{\partial v_e}{\partial x}\right)+\mathcal{D}^2+\frac{\partial u_e}{\partial x}\mathcal{D}\right]\frac{\partial^2\psi}{\partial z^2}+N^2\frac{\partial^2\psi}{\partial x^2}$$
$$-\left(\frac{\partial u_e}{\partial z}\mathcal{D}-\mathcal{D}\frac{\partial u_e}{\partial z}+2\frac{\partial b}{\partial x}\right)\frac{\partial^2\psi}{\partial x\partial z}-\frac{\partial\mathcal{D}}{\partial x}\frac{\partial u_e}{\partial z}\frac{\partial\psi}{\partial z}+\frac{\partial\mathcal{D}}{\partial z}\frac{\partial u_e}{\partial z}\frac{\partial\psi}{\partial x}$$
$$=\left(f^2+\mathcal{D}^2+\frac{\partial\mathcal{D}}{\partial t}\right)\frac{\partial u_e}{\partial z}-\frac{\partial\mathcal{F}_b}{\partial x}, \tag{3.1}$$

where N is the Brunt–Väisälä frequency ($N^2=\partial b/\partial z$) and the stream function ψ is defined as

$$(u,w)=\left(\frac{\partial\psi}{\partial z},-\frac{\partial\psi}{\partial x}\right). \tag{3.2}$$

The vertical velocity is zero on all the boundaries, giving

$$\left.\begin{aligned}\frac{\partial\psi}{\partial x}&=0\quad\text{at } x=\pm L_d\\ \text{and}\qquad\psi&=0\quad\text{at } z=0 \text{ and } z=H.\end{aligned}\right\} \tag{3.3}$$

Equation (3.3) is a free-slip surface boundary condition. A non-slip surface boundary condition ($\partial\psi/\partial z=0$) is ill-posed for an arbitrary forcing term on the right-hand side of equation (3.1) and implies non-zero vertical velocity at the surface. As stated in §3*c*, the diagnosed u from the SGT equations is accurate above the surface layer.

We will now consider the novel structure of equation (3.1). While the SEE is in terms of the geostrophic wind, the SEEBL is in terms of the Ekman-balanced wind. The terms in $\partial v_e/\partial x$ and $\partial u_e/\partial x$ originate from the advection of momentum. The terms in N^2, $\partial b/\partial x$ and F_b represent a full coupling of the boundary layer to the buoyancy equation. In the limit of zero boundary-layer diffusion ($\mathcal{D}\to 0$), the left-hand side of the SEEBL then becomes that of the SEE. SEEs are often solved with the Q-vector forcing on the right-hand side, for example due to frontal deformation [13]. While this is straightforward to include, we choose here to consider just the

role of the boundary-layer forcings in the circulation. Equation (3.1) is discretized using finite differences and solved using a standard sparse matrix solver. The solvability condition for the discretized SEEBL is

$$\left[f\left(f+\frac{\partial v_e}{\partial x}\right)+D^2+\frac{\partial u_e}{\partial x}D\right]N^2-\frac{\partial b}{\partial x}^2>0, \tag{3.4}$$

where D represents the diagonal elements of the discretized $\mathcal{D}$ operator. The presence of the D^2 term makes the discretized SEEBL equation more positive definite than the SEE. While the SEE is degenerate at the equator ($f=0$), the presence of the D terms means that the SEEBL can still diagnose a circulation at the equator.

By applying the balance in equation (2.11) to equations (2.18) and (2.19), we can also diagnose v:

$$(f^2+d^2)v=\left(f^2+d^2+\frac{\partial d}{\partial t}\right)v_e-d\left(u\frac{\partial v_e}{\partial x}+w\frac{\partial v_e}{\partial z}\right)+f\left(u\frac{\partial u_e}{\partial x}+w\frac{\partial u_e}{\partial z}\right), \tag{3.5}$$

where $d(g)=(\partial/\partial z)(K_m(\partial g/\partial z))$, $v=0$ at $z=0$ and $v=v_g$ at $z=H$ (v_g is the geostrophic wind in the y direction).

(a) Other approaches

It is instructive to compare the SEEBL with other approaches in the literature. Thorpe & Nash [13] solved a version of the SEE with an Ekman pumping bottom boundary condition for mid-latitude frontal scenarios. Their formulation did not permit a variable boundary-layer depth or a full representation of the advection of momentum and buoyancy within the boundary layer as allowed in the SEEBL. Smith & Montgomery [14] formulated the SEE in cylindrical polar coordinates for a hurricane boundary layer. However, the balance applied throughout was gradient-wind balance, with no modification for the boundary-layer drag. The boundary-layer friction was applied as a forcing on the right-hand side of the SEE.

The Ekman pumping formula is a popular method of determining the impact of the boundary-layer on the larger scale. Here, Ekman momentum balance is assumed, which in our two-dimensional system appears as the following in the y direction:

$$fu=-\frac{\partial\overline{v'w'}}{\partial z}, \tag{3.6}$$

where $\overline{v'w'}$ is the boundary-layer momentum flux in the y direction. Integrating continuity (equation (2.5)) over the depth of the boundary layer gives the vertical velocity at the top of the boundary layer (w_h). Also assuming that the boundary-layer depth does not vary with x then gives the standard formula:

$$w_h=-\frac{1}{f}\frac{\partial\overline{v'w'}_0}{\partial x}, \tag{3.7}$$

where the subscript 0 indicates the near-surface values. Compared with the SEEBL (equation (3.1)), equation (3.7) neglects the advection of momentum and buoyancy, and the variation of boundary-layer depth in the horizontal. The SEEBL also explicitly includes the surface heat flux via the buoyancy equation (equation (2.4)), unlike the Ekman pumping formula.

4. A baroclinic low-level jet case

In order to demonstrate the performance of the SEEBL, we require a large-scale meteorological case with substantial momentum and buoyancy advection as well as considerable forcing from boundary-layer processes. A baroclinic low-level jet case provides all of these ingredients. Furthermore, the frontal scenario was the original motivation for the SEE [1,2], so it will also be interesting to see how the SEEBL performs in this setting. We first give an example of such a jet from analyses, and then design an idealized version inspired by this case. The idealized case

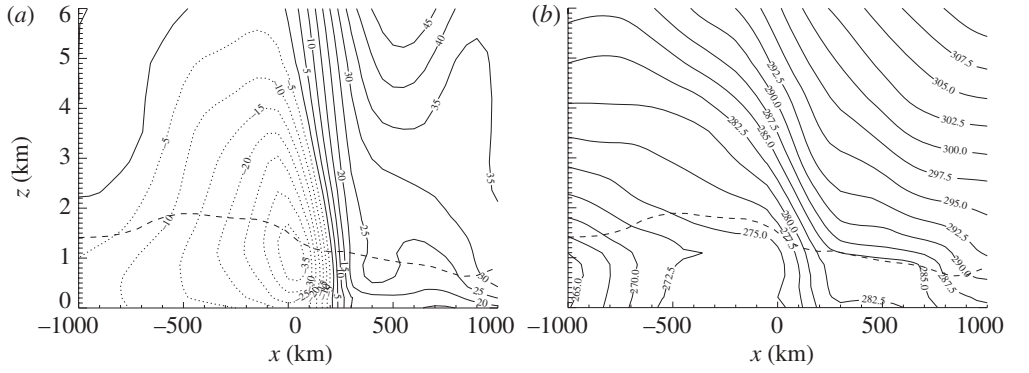

Figure 2. Vertical cross-sections of a mid-latitude cyclone low-level jet from ERA-interim analyses. Cross-sections shown at constant latitude with the origin at latitude 52 N and longitude 41 W for 0Z on 22 December 2008: (*a*) wind in the north–south direction, contour interval 5 m s^{-1}, negative values are represented by dotted lines; (*b*) potential temperature (contour interval 2.5 K). Dashed line represents boundary-layer depth.

consists of an isolated two-dimensional low-level jet and allows a straightforward calculation of all the terms in the SEEBL. We finally show the circulations diagnosed with the SEEBL, along with the sensitivity to the momentum and buoyancy advection terms.

(a) Analysed case

Figure 2 shows ECMWF (European Centre for Medium-Range Weather Forecasts) ERA-interim analyses [15] of a mature mid-latitude cyclone in the West Atlantic on 0Z 22 December 2008, at latitude 52 N. Figure 2*a* shows a significant low-level jet in the centre of the cross-section with a maximum at 1 km height. The jet is associated with the cold conveyor belt. The jet also leans to the left with height consistent with the frontal structure (figure 2*b*). The jet maximum is within the boundary layer. The baroclinicity is indicated by the horizontal gradient of potential temperature (cold to the left, warm to the right). The baroclinic zone within the boundary layer is about 300 km wide. The potential temperature cross-section shows a weakly stratified boundary layer to the left (cold side) of the cold front. The boundary layer is more stratified to the right of the front.

(b) Idealized jet

We aim to reproduce the key features of the analysed low-level wind jet and isolate its impact on the boundary-layer circulation. Of course, our two-dimensional setting will not capture horizontal curvature effects of the analysed case. However, basing the idealized jet on the vertical cross-section will ensure that the scales used are physically realistic. First, we want the jet to lean with height, consistent with a frontal surface. We then want the geostrophic wind to peak near the surface, as this will drive the boundary-layer state. Finally, we want the horizontal shear to be greater on the right side of the jet, and the horizontal and vertical scales of the jet to be consistent with the analysis. These features are achieved by the following geostrophic wind in the y direction:

$$v_g(\hat{x},\hat{z}) = V_0 \exp\left[-\left(\frac{c}{c_j}\right)^2\right] \exp\left(-\frac{\hat{z}}{d_j}\right)\left[1+\tanh\left(-\frac{\hat{x}}{e_j}\right)\right], \tag{4.1}$$

$$\hat{x} = \frac{x}{L_d}, \quad \hat{z} = \frac{z}{H_d} \quad \text{and} \quad c = \hat{x} + \alpha\hat{z},$$

where $V_0 = -30\,\mathrm{m\,s^{-1}}$, $c_j = 0.15$, $d_j = 0.225$, $e_j = 0.0625$ and $\alpha = 0.3$. The domain width ($2L_d$) was 4000 km, and domain height (H_d) 20 km. A horizontal grid length of 31 km and constant vertical

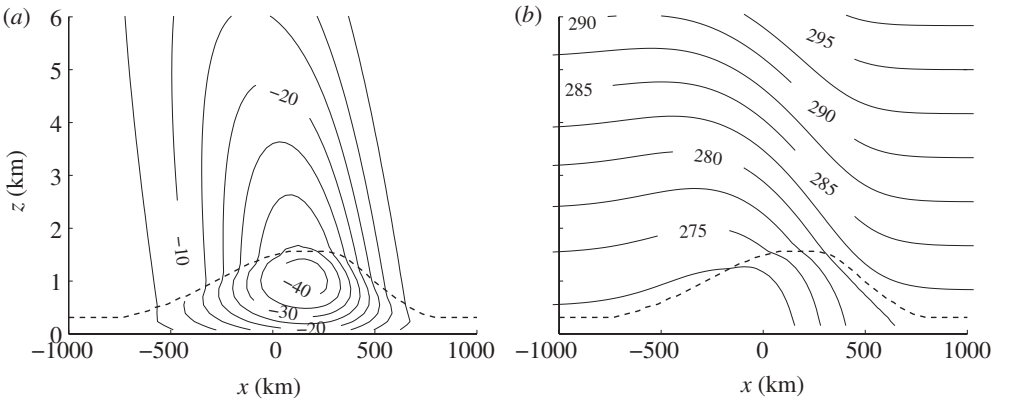

Figure 3. Vertical cross-sections of (*a*) the Ekman-balanced wind in the north–south direction (contour interval 5 m s^{-1}), and (*b*) the potential temperature (contour interval 2.5 K) resulting from the thermal wind balance initialization followed by 6 h of integration of the boundary-layer scheme. Dashed line represents boundary-layer depth.

grid length of 156 m were used. The potential temperature was initialized using thermal wind balance. The initial surface potential temperature was equal to the value at the first grid level above the surface. The boundary-layer parametrization defined in §2 was used, along with the surface exchange scheme of Beljaars & Holtslag [16]. The boundary-layer scheme was integrated with the geostrophic and potential temperature initial conditions. The geostrophic wind and the surface temperature were kept at their initial values throughout the integration. By 6 h, the boundary-layer diffusion settled to an equilibrium value. We determine the Ekman-balanced wind for a given K_m and $\partial\phi/\partial x$ using the matrix inversion method described by Beare & Cullen [6].

Figure 3*a* shows the Ekman-balanced wind in the y direction (v_e) along with the boundary-layer depth. The boundary-layer depth is diagnosed as the height above which the gradient Richardson number is greater than one. The jet peaks at height 1 km, below the boundary-layer top, similar to that in figure 2*a*. The boundary-layer depth increases to a maximum of 1600 m, corresponding to the region of maximum wind speed. This is due to the boundary-layer turbulence being driven by the wind shear. Since we are considering an isolated jet, the variation of boundary-layer depth is more significant than in figure 2. Above the boundary layer, v_e is, by definition, the same as the geostrophic wind. The baroclinic structure (figure 3*b*) above the boundary layer is similar to figure 2*b*. The boundary layer is strongly stratifed to the right, but weakly stratified to the left of the domain. Again, this is similar to figure 2*b*, although it is more well mixed to the left. The horizontal scale of the strongest baroclinic zone (about 300–400 km) is similar to figure 2*b*. The frontal surface in figure 3*b* is less inclined than in figure 2*b*. In summary, although the idealized case does not reproduce the analysed case exactly, many of the key physical features are consistent between the two.

Figure 4*a* shows the Ekman-balanced wind in the x direction (u_e). It is slightly negative near the boundary-layer top and increases to a maximum value of 17 m s^{-1} in the same horizontal location, but below where the low-level jet peaks in figure 3*a*. The profiles of u_e and v_e (figure 3*a*) correspond to the familiar turning of the wind within the boundary layer, with the wind backing when moving down through the boundary layer. The boundary-layer diffusion (K_m, figure 4*b*) follows u_e closely, with a maximum below the middle of the boundary layer.

(c) SEEBL circulations

Figure 5*a* shows the stream function diagnosed using the SEEBL (equation (3.1)). The potential temperature is shown alongside for reference (figure 5*b*). The stream function shows an

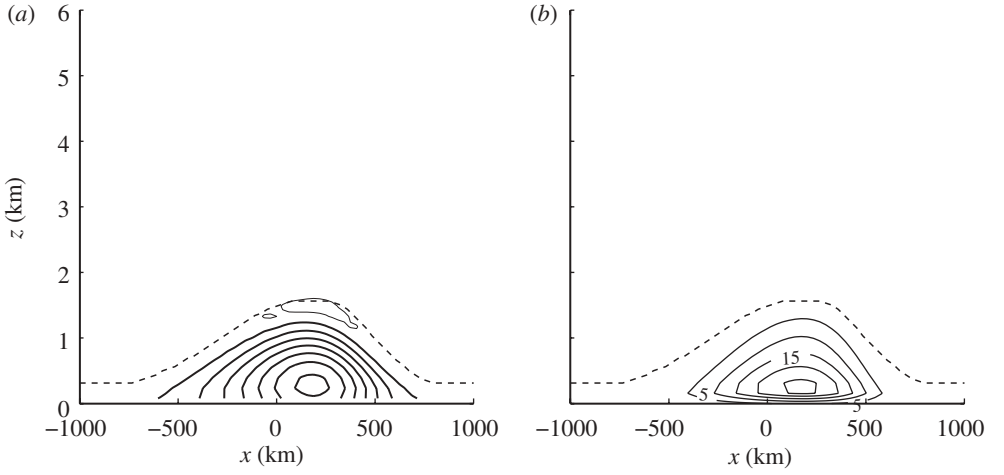

Figure 4. (*a*) Ekman-balanced wind in the *x* direction, u_e (contour interval 2.5 m s^{-1}; bold line, positive; feint line, negative; and zero contour omitted for clarity) and (*b*) boundary-layer momentum diffusivity (contour interval 5 m^2 s^{-1}). Dashed line represents boundary-layer depth.

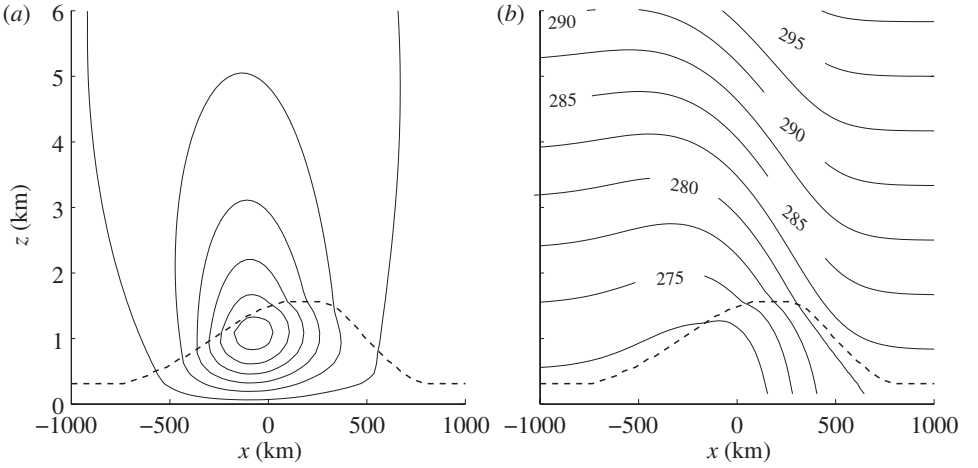

Figure 5. (*a*) Stream function (contour interval 3000 m^2 s^{-1}; outermost contour is 1500) diagnosed by the SEEBL, and (*b*) potential temperature (contour interval 2.5 K). Dashed line represents boundary-layer depth.

anti-clockwise circulation, which is strongest just below the boundary-layer top. There is also a tilt to the left in the axis of the circulation. This is consistent with the effect of baroclinicity seen in SEE calculations [17].

The velocity components diagnosed by the SEEBL are shown in figure 6. Figure 6*a* shows a positive advecting velocity (*u*) within the boundary layer with a negative return flow near the boundary-layer top. The magnitude of the advecting velocity is larger than the Ekman-balanced velocity (figure 4) near the bottom and the top of the boundary layer. The advecting velocity is also phase-shifted by 200 km to the left relative to the Ekman-balanced velocity. The pattern is due to the momentum and buoyancy advection terms along with the enforcement of continuity in the SEEBL.

The vertical velocity pattern (figure 6*b*) accounts for the variation of the boundary-layer depth. There are sloping regions of descent and ascent to the left and right, respectively, of the jet maximum. The region of descent follows the boundary-layer top closely, whereas the region of ascent is slightly below and to the left of the downward sloping boundary-layer

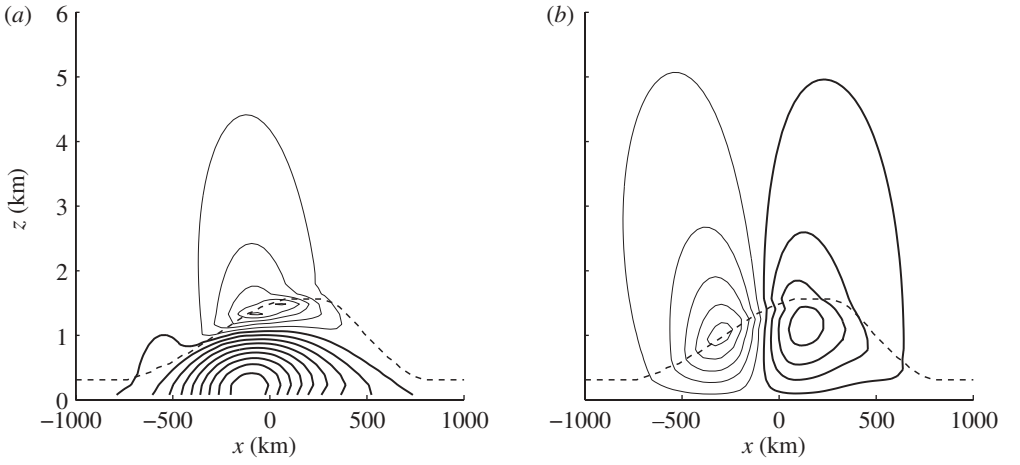

Figure 6. (*a*) Advecting velocity u (contour interval 2.5 m s^{-1}) and (*b*) vertical velocity (contour interval 1 cm s^{-1}) diagnosed by SEEBL. Positive values represented by bold line, negative values by feint line, and zero contour omitted for clarity. Dashed line represents boundary-layer depth.

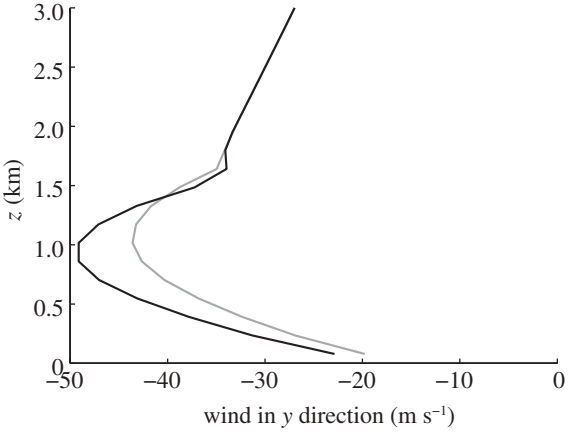

Figure 7. Vertical profiles of v_e (grey) and v (black) at the horizontal location of the jet maximum.

top. The magnitude of the maximum ascent is smaller than the magnitude of the maximum descent: the maximum vertical velocity is 4.1 cm s^{-1} and minimum value is -5.5 cm s^{-1}. In contrast, the Ekman pumping formula (equation (3.7)) diagnoses a maximum vertical velocity of 3.8 cm s^{-1} and minimum value of -2.6 cm s^{-1}. The Ekman pumping thus has the reverse pattern of maximum ascent and maximum descent from the SEEBL, and follows the horizontal vorticity of the jet. However, the SEEBL includes the additional significant effects of a sloping boundary layer, and momentum and buoyancy advection.

Figure 7 compares the advecting velocity v (diagnosed from equation (3.5)) with the Ekman-balanced wind v_e. The v wind has a jet that is significantly larger in magnitude than v_e (by up to 6.5 m s^{-1}). This is a reflection of the momentum advection terms being a significant component of the dynamics (see equation (3.5)). Combined with figure 6*a*, this shows that the full advecting velocity (u, v) has a larger magnitude than the Ekman-balanced velocity (u_e, v_e).

The SEEBL diagnosis was explored further by performing two tests of sensitivity to its coefficients. Figure 8*a* shows the vertical velocity diagnosed by the SEEBL, when the advection of the Ekman-balanced velocity and horizontal buoyancy advection terms are removed

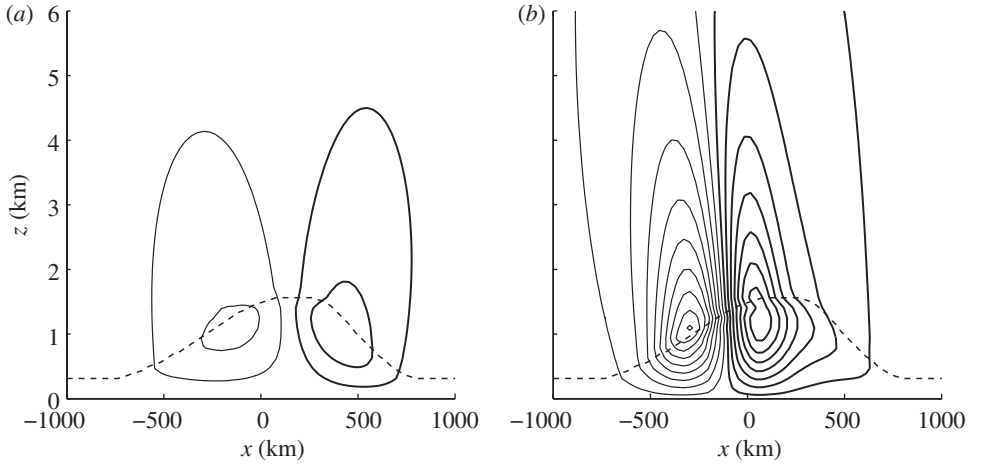

Figure 8. Vertical velocity (contour interval 1 cm s^{-1}), when (*a*) momentum advection and horizontal buoyancy advection terms are neglected in the SEEBL and (*b*) stratification is set to one-quarter of its value in SEEBL. Positive values are represented by bold line, negative values by feint line, and zero contours omitted for clarity. Dashed line represents boundary-layer depth.

(this corresponds to removing the terms in $\partial u_e/\partial x$, $\partial v_e/\partial x$, $\partial^2\psi/\partial x\partial z$, $\partial\psi/\partial x$ and $\partial\psi/\partial z$ in equation (3.1)). The vertical velocity pattern is approximately 50 per cent weaker, and the asymmetry between ascent and descent is now small and slightly reversed. Figure 8*b* shows the effect of reducing the stratification (N^2) by a factor of 4. This amplifies the circulation by a factor of 2, and increases the vertical extent of the circulation (consistent with a scale height for the stream function that varies as $1/N$).

5. Discussion

Ever since the seminal papers of Eliassen [1] and Sawyer [2], an important aspect of dynamical meteorology has been determining the vertical circulations, particulary in frontal zones. The SEE arises out of the semi-geostrophic theory of Hoskins [3]. Several authors [13,14] have incorporated the effects of the boundary layer in the SEE by either the bottom boundary condition or external forcing. However, there has yet to be an explicit treatment of the momentum and thermodynamic balances within the boundary layer, or an accounting of the variation of the boundary-layer depth in space.

In this paper, we described a new methodology for diagnosing circulations forced by the boundary layer coupled to the large-scale dynamics. We derived the analogue of the semi-geostrophic equations for the boundary layer. These were called the SGT equations and used Ekman balance in the place of geostrophic balance. We then formulated a Sawyer–Eliassen type of elliptic equation for the stream function in the vertical plane from the SGT equations, which now explicitly included boundary-layer vertical diffusion (SEEBL).

We showed example numerical solutions of the SEEBL for a baroclinic low-level jet. The circulation from the SEEBL closely followed the significant variation of the boundary-layer depth across the front. The circulation had more descent on the anticyclonic side of the jet than ascent on the cyclonic side; such symmetry was opposite from that predicted by the Ekman pumping. The symmetry of the SEEBL's circulation is also in agreement with Bannon [18], who considered just the boundary-layer momentum budget, and showed that the Ekman pumping overestimates the maximum ascent in cyclonic regions, but underestimates the maximum descent in anti-cyclonic regions. While the Ekman pumping assumes a steady-state momentum balance, the SEEBL also includes advection of momentum and buoyancy, and permits variable

boundary-layer depth. We showed that the net effect of including advection of momentum and horizontal advection of buoyancy was a significant enhancement of the vertical circulation. We also identified vertical advection of buoyancy as a significant control on the depth and strength of the circulation.

The SGT equations have revealed a distinct mechanism for low-level jets from the commonly used inertial oscillation. The jet is enhanced from the Ekman-balanced state owing to the contribution from momentum advection. However, unlike the inertial oscillation jet [19], the jet is 'slaved' to the balanced wind and does not behave in an unbalanced or oscillatory way (figure 7). The SGT equations also provide an explanation of why the low-level jet is found to be significantly ageostrophic [10]. The SGT equations thus provide some new elements of a comprehensive dynamical description of low-level jets.

The benefits of our methodology are not limited to the atmosphere. Samelson & Vallis [20] showed that the frictional planetary geostrophic model has benefit in the oceans. In the same vein, the SEEBL could be adapted to incorporate the interaction of the ocean mixed layer with the ambient dynamics. It could thus prove to be a valuable tool for diagnosing the interaction of the boundary layer with the large-scale dynamics throughout the climate system.

References

1. Eliassen A. 1962 On the vertical circulation in frontal zones. *Geophys. Publ.* **24**, 147–160.
2. Sawyer JS. 1956 The vertical circulation at meteorological fronts and its relation to frontogenesis. *Proc. R. Soc. Lond. A* **234**, 346–362. (doi:10.1098/rspa.1956.0039)
3. Hoskins BJ. 1975 The geostrophic momentum approximation and semi-geostrophic equations. *J. Atmos. Sci.* **33**, 233–242. (doi:10.1175/1520-0469(1975)032<0233:TGMAAT>2.0.CO;2)
4. Beare RJ. 2007 Boundary layer mechanisms in extratropical cyclones. *Q. J. R. Meteorol. Soc.* **133**, 503–515. (doi:10.1002/qj.30)
5. Back LE, Bretherton CS. 2009 On the relationship between SST gradients, boundary layer winds, and convergence over the tropical oceans. *J. Clim.* **22**, 4182–4196. (doi:10.1175/2009JCLI2392.1)
6. Beare RJ, Cullen MJP. 2010 A semi-geostrophic model incorporating well-mixed boundary layers. *Q. J. R. Meteorol. Soc.* **136**, 906–917. (doi:10.1002/qj.612)
7. Beare RJ, Cullen MJP. 2012 Balanced models of boundary-layer convergence. *Q. J. R. Meteorol. Soc.* **138**, 1452–1464. (doi:10.1002/qj.1877)
8. Clark PA, Browning KA, Wang C. 2005 The sting at the end of the tail: model diagnostics of fine-scale three-dimensional structure of the cloud head. *Q. J. R. Meteorol. Soc.* **131**, 2263–2292. (doi:10.1256/qj.04.36)
9. Chen GT-J, Wang C-C, Lin DT-W. 2005 Characteristics of low-level jets over Northern Taiwan in Mei-Yu season and their relationship to heavy rain events. *Mon. Weather Rev.* **133**, 20–43. (doi:10.1175/MWR-2813.1)
10. Akiyama T. 1973 Ageostrophic low level jet stream in the Baiu season associated with heavy rainfalls over the sea area. *J. Meteorol. Soc. Jpn.* **51**, 205–208. (https://www.jstage.jst.go.jp/article/jmsj1965/51/3/51_3_205/_pdf)
11. Louis JF. 1979 A parametric model of vertical eddy fluxes in the atmosphere. *Bound. Layer Meteorol.* **17**, 187–202. (doi:10.1007/BF00117978)
12. Pedlosky J. 1987 *Geophysical fluid dynamics*, 2nd edn. Berlin, Germany: Springer.
13. Thorpe AJ, Nash CA. 1984 Convective and boundary layer parametrizations in a diagnostic model of atmospheric fronts. *Q. J. R. Meteorol. Soc.* **110**, 443–466. (doi:10.1002/qj.49711046409)
14. Smith RK, Montgomery MT. 2008 Balanced boundary layers used in hurricane models. *Q. J. R. Meteorol. Soc.* **134**, 1385–1395. (doi:10.1002/qj.296)
15. Dee DP *et al.* 2011 The ERA-interim reanalysis: configuration and performance of the data assimilation system. *Q. J. R. Meteorol. Soc.* **137**, 553–597. (doi:10.1002/qj.828)
16. Beljaars ACM, Holtslag AAM. 1991 Flux parameterization over land surfaces for atmospheric models. *J. Appl. Meteorol.* **30**, 327–341. (doi:10.1175/1520-0450(1991)030<0327:FPOLSF>2.0.CO;2)

17. Hakim GJ, Keyser D. 2001 Canonical frontal circulation patterns in terms of Green's functions for the Sawyer–Eliassen equation. *Q. J. R. Meteorol. Soc.* **127**, 1795–1814. (doi:10.1002/qj.49712757517)
18. Bannon PR. 1998 A comparison of Ekman pumping in approximate models of the accelerating planetary boundary layer. *J. Atmos. Sci.* **55**, 1446–1451. (doi:10.1175/1520-0469(1998)055<1446:ACOEPI>2.0.CO;2)
19. Ostdiek V, Blumen W. 1997 A dynamic trio: inertial oscillation, deformation frontogenesis. *J. Atmos. Sci.* **54**, 1490–1502. (doi:10.1175/1520-0469(1997)054<1490:ADTIOD>2.0.CO;2)
20. Samelson RM, Vallis GK. 1997 A simple friction and diffusion scheme for planetary geostrophic basin models. *J. Phys. Oceanogr.* **27**, 186–194. (doi:10.1175/1520-0485(1997)027<0186:ASFADS>2.0.CO;2)